Composition Fluctuations, Phase Behavior, and Complex Formation in Poly(vinyl methyl ether)/D_2O Investigated by Small-Angle Neutron Scattering

Erik Nies,*,†,‡ Aissa Ramzi,†,§ Hugo Berghmans,‡ Ting Li,‡,∥ Richard K. Heenan,⊥ and Stephen M. King⊥

Laboratory of Polymer Technology, Eindhoven University of Technology, P.O.Box 513, 5600MB Eindhoven, The Netherlands, Polymer Research Division, Department of Chemistry, Katholieke Universiteit Leuven, Celestijnenlaan 200F, B-3001 Heverlee, Belgium, State Key Laboratory of Polymer Physics & Chemistry, Center for Molecular Science, Institute of Chemistry, Chinese Academy of Sciences, Zhongguancun, Beijing 100080, Peoples' Republic of China, and ISIS Facility, Rutherford Appleton Laboratory, Chilton, Didcot, Oxfordshire OX11 0QX, U.K.

Received July 15, 2004; Revised Manuscript Received October 29, 2004

ABSTRACT: Small-angle neutron scattering measurements are presented as a function of temperature and composition for homogeneous mixtures of poly(methyl vinyl ether) and D_2O. The experimental data are analyzed to give values of the second-order compositional derivative of the Gibbs energy and the Ornstein−Zernike correlation length. From the experimental data the LCST spinodal temperatures are estimated and values for the parameters in a temperature- and composition-dependent extended Flory−Huggins (F−H) interaction function are determined. Using the extended interaction function the predicted miscibility behavior is in qualitative agreement with the experimental data, and importantly, the remarkable bimodal phase behavior is predicted. In the composition interval $0.75 \leq w_{PVME} \leq 0.85$ the Ornstein−Zernike correlation lengths follow the mean field sum rule, i.e., $\xi^2 \approx [(\partial^2 \Delta G/(NkT))/\partial \phi_2{}^2]^{-1}$. However, in the composition range $0.1 \leq w_{PVME} \leq 0.7$ the correlation lengths are still proportional to the second-order compositional derivative of the Gibbs energy but the data cluster on separate power laws with distinct exponents. Finally, the experimental data do not support the existence of a stable molecular complex at the investigated temperatures and compositions. Even at the lowest investigated temperature the energy required to induce typical Ornstein−Zernike-like concentration fluctuations is smaller than the thermal energy. Therefore, in the investigated temperature interval it must be concluded that the strength of the specific interactions between D_2O and PVME is too weak to speak about complex formation.

Introduction

Aqueous polymer solutions frequently show the occurrence of LCST and closed loop phase behavior. This is not really surprising as it is characteristic of polymer solutions that exhibit hydrogen bonding.[1−5] Representative examples are aqueous solutions of poly(ethylene oxide),[6] poly(*N*-vinylpyrollidone),[7] poly(*N*-vinyl caprolactam),[8] and poly(vinyl alcohol)[9] to name a few. In these polymer solutions and small molecule mixtures alike orientation-dependent or saturation interactions play a key factor in the occurrence of LCST and closed loop phase behavior and lead to flat and wide LCST miscibility gaps encompassing the largest part of the composition range, certainly in comparison with UCST behavior but also in comparison with LCST behavior arising from, e.g., compressibility effects.[10−13]

Aqueous solutions of PVME are in this respect not special or remarkable and exhibit a wide LCST miscibility gap nearly covering the full composition range (see Figure 6b for the complete phase diagram).[14,15] However, unusual for the LCST phase behavior in PVME/D_2O and PVME/H_2O is the bimodality of the liquid−liquid (L−L) miscibility gap[14,16] with two stable critical points.[17] The stable critical condition in the dilute or semidilute regime of polymer composition is governed by the combinatorial entropy contribution to the Gibbs energy and changes with molar mass as expected from the classic Flory−Huggins theory and other more advanced theories available in the literature.[18−21] The second stable critical point at high polymer concentrations practically does not change with molar mass, yielding—in the limit of infinite chain length—a nonzero limiting critical concentration.[17] More recently an indication of a bimodal LCST spinodal in poly(ethylene oxide)/D_2O has been reported.[22] Although not commented on by the authors, the experimental spinodal curve extrapolated from SANS data shows a bimodal shape just as in the case of PVME/H_2O and PVME/D_2O discussed in this article.

Apart from the high-temperature phase behavior, aqueous polymer solutions also have been investigated at temperatures below the normal freezing point of water.[23−27] In several systems it is found that water ceases to crystallize at sufficiently high polymer concentration. For instance, in aqueous solutions of poly(*N*-vinyl pyrrolidone) this is probably merely an effect of vitrification of the highly concentrated and viscous polymer solutions before crystallization of water can occur.[23,24] However, in aqueous mixtures of PVME this is not necessarily the case since the glass-transition temperature of PVME is quite low (T_g ca. −30 °C) and

* To whom correspondence should be addressed. E-mail: e.l.f.nies@tue.nl.
† Eindhoven University of Technology.
‡ Katholieke Universiteit Leuven.
§ Present address: Utrecht University, Department of Pharmaceutics, Sorbonnelaan 16, P.O. Box 80082, 3508 TB, Utrecht, The Netherlands.
∥ Chinese Academy of Sciences.
⊥ ISIS Facility, Rutherford Appleton Laboratory.

10.1021/ma0485641 CCC: $30.25
Published on Web 01/11/2005

vitrification probably plays no role for the compositions and temperatures at which crystallization is stopped.[25,26] In these non-crystallizable solutions it is assumed that a polymer/solvent complex is formed in which water molecules are bound to the polymer chain. Depending on the investigated property, polymer/water complexes containing 2−5 molecules of water have been suggested.[25,28,29]

The complexity of the phase behavior puts a challenge to its molecular understanding and theoretical description and prediction. One possible approach is to incorporate the specific interactions in the theoretical description as is done in the statistical association fluid theory[30] or the theoretical approaches of, e.g., Wertheim,[31] Dormidontova,[3] and Veytsman.[32] In another approach, taken in this article, emphasis is put on the experimental (thermodynamical) observations and semiphenomenological modeling of the complicated behavior with a (limited) set of fitting parameters.[33,34] In this phenomenological approach one can start from, e.g., the simple theoretical thermodynamic expression of Flory and Huggins for the Gibbs free energy amended with a semiempirical temperature- and composition-dependent Flory−Huggins (FH) interaction parameter that is capable of describing the relevant aspects of the observed thermodynamic behavior. For instance, the semiphenomenological approach served as a starting point to catalog different forms of complex LCST phase behavior according to Types 1, 2, and 3.[17] 'Type 1' is the classical Flory−Huggins behavior for which the L−L critical composition shifts to lower polymer concentrations with increasing polymer molar mass. 'Type 2' demixing behavior stands for liquid−liquid demixing behavior with critical composition that hardly changes with polymer molar mass and remains nonzero, even for infinite molar mass. 'Type 3' behavior concerns bimodal L−L demixing behavior with two stable critical points, one at low polymer concentration with a classic Type 1 FH behavior and a second one at high polymer concentration as for Type 2 behavior.[17] Although this phenomenological approach provides no real insight in the underlying molecular interactions and mechanisms responsible for the observed thermodynamic behavior, it certainly makes it possible to predict, for instance, the behavior of polymer networks and gels in terms of the behavior of the corresponding linear polymer.[14] A drawback of this semiphenomenological approach is that a rather large number of phenomenological parameters is required in the temperature- and composition-dependent interaction parameter, especially to model the complicated bimodal phase behavior. In practice, the parameters are derived from the measured phase behavior such as cloud point data, spinodal data, or melting point data. This complicates the estimation of the parameters in the model as the thermodynamic variables are coupled in transition points. To estimate the phenomenological parameters it would be preferable to have experimental data available in which the thermodynamic variables pressure, temperature, and composition can be varied independently. Light, X-ray, and neutron scattering experiments allow us to perform such measurements in the homogeneous region of the phase diagram since the scattering cross-section measured in a scattering experiment is directly proportional to the second-order compositional derivative of the Gibbs energy of the system.[35,36] Light scattering and X-ray scattering are in this case less suited: the contrast for X-rays is quite low in the system PVME/water or PVME/D_2O, and the preparation of highly viscous polymer mixtures of sufficient optical quality for light scattering is far from trivial.

In this article we report SANS measurements covering the whole composition range in the homogeneous part of the phase diagram, bounded by the LCST at high temperature and the crystallization/melting of D_2O at low temperature (see Figure 6b). A few SANS studies on the properties of the homogeneous bulk system PVME/D_2O have appeared in the literature.[37,38] The authors focused on semidilute solutions of PVME in D_2O and methanol−D_2O mixtures in the poor solvent regime. Moreover, in two SANS studies of PVME/D_2O the composition and properties of the structure of PVME layers adsorbed at the water/air interface and the effect of the addition of PVME and salts on the structure and the tactoid-to-gel phase transition temperature of the clay *N*-butylammonium vermiculite were addressed.[39,40]

The SANS data collected in this investigation serve to provide values for the polynomial coefficients in a semiphenomenological Flory−Huggins (FH) interaction parameter depending on temperature and composition. With this extended FH interaction parameter the LCST phase behavior is predicted using the parameter values derived from the SANS data. Apart from this thermodynamic use the data give us the opportunity to shed further light on the issue of polymer/solvent complex formation.

In the next section chemicals and experimental techniques are described. In the theoretical section the relationship between SANS scattering cross-sections, concentration fluctuation theory, and thermodynamic properties is briefly highlighted. These relationships are then specified in a Flory−Huggins expression for the Gibbs energy, amended with a composition- and temperature-dependent interaction parameter. The results of the current investigation are presented and discussed in the Results and Discussion, and finally some conclusions and suggestions for further research are presented in the Conclusions and Outlook.

Experimental Section

Materials and Mixtures Preparation. Poly(vinyl methyl ether) (PVME, $(CH_2CHOCH_3)_n$) dissolved in water (mass fraction of PVME, $w_{PVME} = 0.5$) was purchased from Sigma-Aldrich. The mixture was diluted to $w_{PVME} = 0.3$ and heated to ca. 50 °C to induce liquid−liquid phase separation. The phase lean in polymer was removed, and the phase rich in polymer was further dried at 60 °C under vacuum for 2 days. The dried PVME was used in the further preparation of binary polymer mixtures either with D_2O and toluene-d_8. Deuterium oxide (D_2O) (purity 99.95%) and deuterated toluene-d_8 (C_6D_5-CD_3, purity 99.5%) purchased from Merck are used without further purification.

In the composition range $0.1 \leq w_{PMVE} \leq 0.85$ mixtures of PVME and D_2O are prepared by adding appropriate amounts of polymer and solvent. Mixture compositions are expressed in PVME mass fraction w_{PVME}. These mixtures were allowed to homogenize at room temperatures in closed recipients for periods up to 2 months for the highest polymer concentrations. Regularly the mixtures were mechanically mixed in the recipient. We do not consider higher concentrations $w_{PVME} > 0.85$ in this study because samples of very good quality could not be prepared (some air bubbles were unavoidable).

Dilute solutions of PVME in D_2O and toluene-d_8 ($w_{PVME} = 0.001$ and 0.005) were prepared by mixing appropriate amounts of polymer and solvent.

Small-Angle Neutron Scattering (SANS) Measurements. Small-angle neutron scattering (SANS) experiments

were performed on the LOQ instrument at the ISIS pulsed neutron source, Rutherford Appleton Laboratory, Didcot, U.K.[41] The range of wavelengths used was $2.2 \leq \lambda \leq 10$ at 25 Hz, corresponding to the range $0.006 \leq q \leq 1.49$ Å^{-1} in scattering vector amplitude $q = 4\pi \sin(\theta/2)/\lambda$. The beam size at the sample position was 10 mm. Scattering intensities were collected on two 2D detectors. Details about the detectors can be found elsewhere.[41] The two detectors have slightly different q-resolution, and because the high-angle detector cannot be placed in the path of the transmitted beam, it is not possible to compensate for what it records for differences in detection efficiency to the same precision (particularly with samples that contain more hydrogen). These two factors manifest themselves in the SANS data presented here as a change in the spacing of the data points and a slight mismatch in incoherent baseline level, respectively.

The raw scattering data were treated according to standard reduction procedures using the 'COLETTE' program developed at ISIS.[42] Overhead runs consisting of the empty cell and transmission runs of the empty and filled cell were also performed. As expected, in the limited temperature interval studied the transmissions of the samples do not vary noticeably with temperature within experimental accuracy and the transmission measurement time (about 7 min). Therefore, the transmission of each sample composition was only measured at room temperature and used in the data reduction for all temperatures. Raw data were divided by the sample thickness and the measured transmission and corrected for detector efficiency. The scattering cross-sections were obtained by circularly averaging the isotropic scattering datasets. Subsequently, the corrected scattering cross-section recorded from the empty sample cuvette was subtracted from the scattering data. To convert the data to absolute cross-sections, expressed in cm^{-1}, the scattered intensities were multiplied by a predetermined calibration factor. Details are discussed elsewhere.[41]

Samples were contained in quartz glass cells (purchased from Starna and Hellma). Dilute solutions were placed in closed cells of 2 mm path length, closed with a Teflon stopper. The highly viscous concentrated mixtures were placed in demountable but sealed cells with a 1 mm path length to reduce incoherent scattering effects from hydrogen atoms. SANS measurements were performed as a function of mixture composition and temperature. The exposure time at each temperature was 1 h, and after attaining a new measuring temperature an equilibration time of ca. 20 min was taken into account.

Theoretical Section

Scattering Cross-Sections Due to Concentration Fluctuations. Here we interpret the experimental scattering cross-sections according to the concentration fluctuation theory initiated by Smoluchowski,[43] Einstein,[44] and Debye.[35] The recorded absolute scattering cross-sections of the samples contain an incoherent contribution carrying no structural information and coherent contributions due to density fluctuations and concentration fluctuations. The pure hydrogenated PVME in particular has considerable incoherent and, most likely, inelastic scattering contributions. To obtain the scattering related to the concentration fluctuations in binary mixtures of solvent and polymer (PVME), the incoherent scattering largely caused by the hydrogenated material and the coherent scattering caused by density fluctuations is removed from the measured signal by subtracting the scattering of the pure components in the appropriate volume ratio[45]

$$\left.\frac{\partial\sigma}{\partial\Omega}(q)\right|_{\text{conc}} = \left.\frac{\partial\sigma}{\partial\Omega}(q)\right|_{\text{total}} - \phi_{\text{solvent}}\left.\frac{\partial\sigma}{\partial\Omega}(q)\right|_{\text{solvent}} - \phi_{\text{PVME}}\left.\frac{\partial\sigma}{\partial\Omega}(q)\right|_{\text{PVME}} \quad (1)$$

where $\partial\sigma/\partial\Omega(q)|_X$ is the absolute coherent scattering cross-section due to concentration fluctuations (X = conc), the total scattering cross-section (X = total), the total scattering cross-section of the solvent (X = D_2O or toluene-d_8) and of PVME (X = PVME) and ϕ_i is the volume fraction of component i in the mixture.

Of course, in practice, the subtraction in eq 1 will not be perfect due to experimental uncertainties in the scattered intensities and in the volume fractions and a residual background signal may remain; hence, the experimental scattering cross-section is presented by

$$\left.\frac{\partial\sigma}{\partial\Omega}(q)\right|_{\text{conc,exp}} = \left.\frac{\partial\sigma}{\partial\Omega}(q)\right|_{\text{conc}} + B \quad (2)$$

with B being a (small) residual q-independent background intensity.

The volume fractions of the mixture components are calculated from the mass fraction and the assumption that mixing is not accompanied by volume changes (see Supporting Information).

Scattering Cross-Section from Concentration Fluctuation Theory. The absolute scattering cross-section due to concentration fluctuations in a binary mixture is according to the fluctuation theory given by[35,36,45]

$$\left.\frac{\partial\sigma}{\partial\Omega}(q)\right|_{\text{conc}} = \frac{\left.\frac{\partial\sigma}{\partial\Omega}(q=0)\right|_{\text{conc}}}{(1+(\xi q)^2)} = \frac{\bar{b}^2}{V_0}\frac{\left(\frac{\partial^2\Delta G/(NkT)}{\partial{\phi_2}^2}\right)^{-1}}{(1+(\xi q)^2)} \quad (3)$$

with $\partial\sigma/\partial\Omega(q=0)|_{\text{conc}}$ being the scattering cross-section in the forward direction and ξ the correlation length [Å], $\bar{b} = V_0(b_1/V_1 - b_2/V_2)$ the contrast factor, V_0 the volume of the unit cell, V_1 (V_2) the volume of a molecule of the solvent (component 1) (polymer, component 2), b_1 (b_2) the neutron scattering length of species 1 (2), $\Delta G/N$ the free enthalpy of mixing per unit cell, N the number of unit cells, k Boltzmann's constant, and T the absolute temperature.

The neutron scattering length, b_M, of a molecule M consisting of atoms of type i is readily calculated from[36,46]

$$b_M = \sum_i b_i \quad (4)$$

where b_i is the neutron scattering length of an atom of type i taken from the literature.[46] For polymer chains it is only necessary to calculate b_M for one repeat unit. The scattering length densities of PVME, toluene-d_8, and D_2O are summarized in the Supporting Information.

The compositional curvature is also related to the average amplitude of thermal composition fluctuations in the mixture, which for a binary mixture becomes[47−49]

$$\langle\Delta{\phi_2}^2\rangle = \left(\frac{\partial^2\Delta G/(NkT)}{\partial{\phi_2}^2}\right)^{-1} \quad (5)$$

Finally, for sufficiently dilute solutions of a polydisperse polymer the scattering arises from isolated polymer chains. In this case a plot of

$$\frac{{V_o}^2}{\bar{b}^2\phi_2}\left.\frac{\partial\sigma}{\partial\Omega}(q)\right|_{\text{conc,exp}} = \frac{M_{w,2}}{(1+\langle s^2\rangle_z q^2/3)} + B \quad (6)$$

Table 1. Estimated Residual Background, *B*, Molar Mass, and Radius of Gyration of PVME in D_2O and Toluene-d_8. Results in the Last Column Are Obtained Assuming that a Complex between PVME and D_2O Is Formed Containing Two D_2O Molecules Per Repeating Unit of the Polymer

	PVME/D_2O	PVME/toluene-d_8	PVME-$(D_2O)_2$/D_2O
$\partial\sigma/\partial\Omega(q=0)/\phi_{PVME}$ (cm^{-1})	124 ± 6	104 ± 6	123.7 ± 6
M_w (kg mol^{-1})	21 ± 2	23.0 ± 2	59 ± 3
B (cm^{-1})	-0.01 ± 0.2	-0.0007 ± 0.0002	
no. of repeating units	362 ± 26	396 ± 34	601 ± 31
$\sqrt{\langle s^2\rangle_z}$ (nm)	13.4 ± 0.5	13.0 ± 0.5	13.4 ± 0.5
ξ (nm)	4.45 ± 0.2	4.33 ± 0.2	4.45 ± 0.2

should give rise to a universal curve independent of concentration from which the weight-average molar mass, M_w, and the z-average square radius of gyration, $\langle s^2\rangle_z$, can be determined.

Spinodal Conditions and Scattered Intensity. At the stability limit or spinodal condition the curvature of the Gibbs energy becomes zero.[50] Without making reference to any (molecular) theory for the Gibbs energy of mixing and ignoring the gradient energy contribution and nonclassical behavior, which both only become important close to the stability limit,[35] a mean field estimate of the spinodal temperature at a particular composition can be determined from the extrapolation as a function of the temperature or inverse temperature of $\partial^2[\Delta G/(NkT)]/\partial\phi_2{}^2$ or the inverse of the forward scattering cross-sections $(\partial\sigma/\partial\Omega(q=0)|_{conc})^{-1}$ to zero value.

Amended Flory–Huggins Gibbs Free Energy of Mixing Expression. Further information about the thermodynamics can be obtained when we use a specific theoretical model for the Gibbs energy. Here we will adopt the classic Flory–Huggins lattice theory expression for the Gibbs energy amended with an interaction function dependent on temperature and mixture composition.[17,50]

The main equation of this theory describes the free enthalpy of mixing per lattice site (unit cell) of two monodisperse components as follows

$$\frac{\Delta G}{NkT} = \frac{\phi_1}{s_1}\ln\phi_1 + \frac{\phi_2}{s_2}\ln\phi_2 + \Gamma(\phi_2,T) = \frac{\phi_1}{s_1}\ln\phi_1 + \frac{\phi_2}{s_2}\ln\phi_2 + \phi_1\phi_2 g(\phi_2,T) \quad (7)$$

with $\phi_2(\phi_1)$ being the volume fraction of polymer (solvent), s_2 (s_1) the relative chain length or number of unit lattice cells taken by a molecule of component 2 (1), $\Gamma(\phi_2,T)$ the Flory Huggins interaction function, and $g(\phi_2,T)$, the extended F–H interaction parameter defined by the second equality assumed to be a polynomial in concentration and temperature. The relative chain lengths s_i in eq 7 are calculated from $s_i = M_i/\rho_i V_l N_A$ with being M_i the molar mass, ρ_i the density of component i, V_l the volume of a lattice unit cell, and N_A Avogadro's number.

From the analysis of the experimental results presented below it turned out that at least a cubic polynomial function was needed to get an acceptable fit of the data

$$g(\phi_2,T) = \sum_{l=0}^{l_{max}=3} g_l(T)\phi_2{}^l \quad (8a)$$

In eq 8a the different coefficients g_l depend only on temperature. A typical temperature dependence capable of describing a large temperature domain is[50]

$$g_l = g_{l0} + \frac{g_{l1}}{T} + g_{l2}T \quad (8b)$$

where g_{l0}, g_{l1}, and g_{l2} are constants.

At higher polymer compositions the full expression resulting from combining eqs 3, 7, and 8 must be used in the evaluation. In this case the experimental scattering cross-sections for concentration fluctuations make it possible to determine the coefficients in the extended Flory–Huggins interaction parameter function defined in eq 8.

Results and Discussion

Molar Mass and Radius of Gyration of PVME. The pure components PVME, D_2O, and toluene-d_8 as well as dilute solutions of PVME in D_2O and toluene-d_8 ($w_{PVME} = 0.001$ and $w_{PVME} = 0.005$, respectively) were measured at 20 °C. The absolute scattering cross-sections of dilute solutions of PVME in D_2O and in toluene-d_8 normalized to the polymer volume fraction were analyzed according to eq 6 to determine M_w and $\langle s^2\rangle_z$. The forward scattering cross-sections and the correlation lengths lead to values of M_w, $\langle s^2\rangle_z$, and B which are summarized in Table 1 together with their estimated accuracy from the uncertainties in the scattering cross-sections. The values of M_w and $\langle s^2\rangle_z$ in D_2O and toluene-d_8 are equal within experimental error.

Dilute Solutions and Complex Formation. The formation of molecular complexes between PVME and D_2O has been discussed on several occasions in the literature. The number of water molecules per PVME repeating unit in the molecular complex varies from 2 to ca. 5 depending on the literature source and on the experimental method used to investigate complex formation.[25–29] For example, from IR data Maeda et al. concluded that depending on the mixture composition, complexes containing 2.7 or 5 water molecules are formed.[27–29] On the other hand, from the course of the melting point of water with polymer concentration a molecular complex of $2H_2O$ (D_2O) molecules per PVME repeating unit has been proposed by Meeussen et al.[25] This molecular complex P(VME/$(H_2O)_2$) was assumed to remain stable as long as the nucleation of water does not occur.[26] In the case that the water molecules are strongly bonded to the PVME backbone, the complexed molecule can be considered as a new component with its proper density, molar mass, and scattering length. If we assume that two molecules of D_2O are complexed with a PVME repeating unit, the molar mass of this unit is $M_{complex} = (2 \times M_{D_2O} + M_{PVME,repeating\ unit}) = 98.134$ g·mol^{-1}. An estimate of the molar volume of the complex can be made based on the additivity of the PVME and

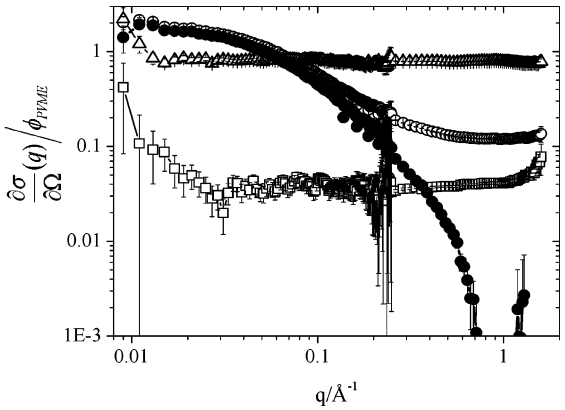

Figure 1. Plot of the scattering cross-section $\partial\sigma/\partial\Omega(q)|_X$ and estimated experimental uncertainties vs q for PVME/D_2O $w_{PVME} = 0.10$. The solid lines connecting the data points are to guide the eye. Plots of the pure components D_2O and PVME $\partial\sigma/\partial\Omega(q)|_{D2O}$ (□), $\partial\sigma/\partial\Omega(q)|_{PVME}$ (△); plot of the mixture data $\partial\sigma/\partial\Omega(q)|_{total}$ (○), and plot of the scattering cross-section for concentration fluctuations according to eq 1 $\partial\sigma/\partial\Omega(q)|_{conc,exp}$ (●).

D_2O volumes: $V_{complex} = (2 \times M_{D_2O}/\rho_{D_2O} + M_{PVME,repeating\ unit}/\rho_{PVME}) = 92.79\ cm^3 \cdot mol^{-1}$. The density of the complex is then $M_{complex}/V_{complex} = 1.0576\ g \cdot cm^{-3}$.

These data together with the scattering lengths of D_2O and PVME were used to calculate the scattering length density of the complex. Finally, from the forward scattering cross-section the molar mass of the complex and the number of repeating units [VME/$(H_2O)_2$] in the chain are calculated; these results are collected in the last column of Table 1. The assumption that a stable complex is formed that can be treated as a proper component leads to a molar mass of the PVME polymer much larger than the molar mass derived from the direct measurement in toluene-d_8 where certainly no complex is formed. Furthermore, agreement between the experimental data for PVME in D_2O and toluene-d_8 treated as normal solutions indicates that surely no strong complex is formed between PVME and D_2O. Hence, for the conditions of the SANS measurements, i.e., in dilute solutions at 20 °C, the experimental data do not support the existence of a stable molecular complex. Further discussion of complex formation in the concentrated mixtures is given below.

Concentrated Mixtures of PVME/D_2O. *Experimental SANS Scattering Cross-Sections.* Eight compositions of PVME in D_2O covering the whole concentration range $0.1 \le w_{PVME} \le 0.85$ were measured at different temperatures ranging from 9 to 35 °C. All experimental scattering data were analyzed using the Ornstein–Zernike (OZ) equation (eq 3), and the forward-scattered intensity $\partial\sigma/\partial\Omega(q = 0)|_{conc}$, the correlation length, and the residual background B were determined at each composition and temperature. The numerical values of the fitting parameters for all compositions and temperatures are provided as Supporting Information accompanying this paper. In Figure 1 a typical example is presented of the total scattering cross-sections of pure components (PVME and D_2O) and mixtures (PVME/D_2O) and the calculated cross-section due to concentration fluctuations for a mixture with $w_{PVME} = 0.1$. The results of $w_{PVME} = 0.1$ are representative for the mixtures in the composition range $0 \le w_{PVME} \le 0.7$. In this composition interval the subtraction procedure to obtain the cross-section due to concentration fluctuations is quite reliable: the residual background intensity derived from fitting the data is 2–3 orders of magnitude smaller than the maximal scattering cross-section and the scattering cross-sections decay to zero as expected from the OZ theory for concentration fluctuations. For concentrations in the interval $0.7 \le w_{PVME} \le 0.85$ the subtraction procedure is not always perfect as in a few cases larger residual background intensity remains. Nevertheless, in practically all cases the values of the background B are still acceptable (≤5% of the forward scattering intensity).

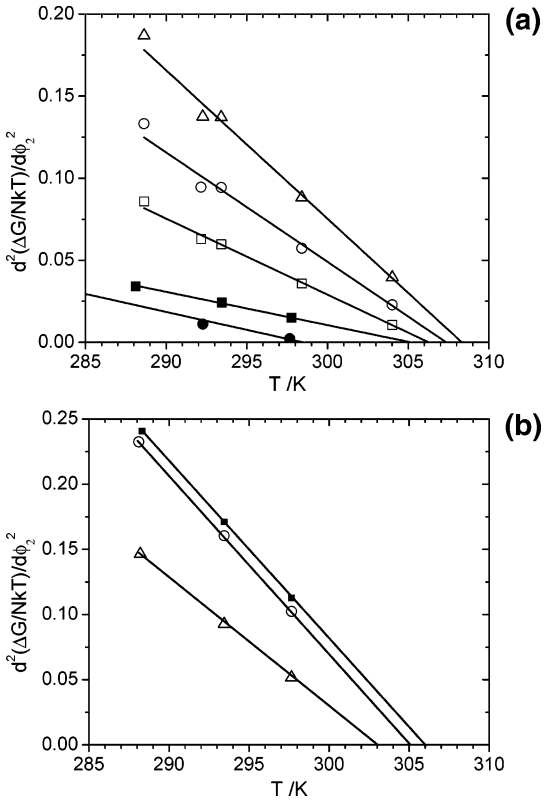

Figure 2. Plot of $\partial^2[\Delta G/(NkT)]/\partial\phi_2^2$ vs T at given mixture composition. The extrapolated temperature at $\partial^2[\Delta G/(NkT)]/\partial\phi_2^2 = 0$ is the spinodal temperature T_{spin}. The error bars are often smaller than the size of the symbols and are not shown. (a) $w_{PVME} = 0.80$, ■; $w_{PVME} = 0.70$, ●; $w_{PVME} = 0.10$, □; $w_{PVME} = 0.20$, ○; $w_{PVME} = 0.30$, △ and (b) $w_{PVME} = 0.60$, △; $w_{PVME} = 0.50$, ○; $w_{PVME} = 0.40$, ■.

Spinodal Conditions. Independent of any (molecular) model for the Gibbs energy (of mixing) the spinodal temperatures can be determined from the forward scattering cross-sections. For each concentration the values of $\partial^2[\Delta G/(NkT)]/\partial\phi_2^2$ (or $(\partial\sigma/\partial\Omega(q = 0)|_{conc})^{-1}$) are plotted versus T as presented in Figure 2. (The alternative procedure consists of plotting $\partial^2[\Delta G/(NkT)]/\partial\phi_2^2$ $(\partial\sigma/\partial\Omega(q = 0)|_{conc})^{-1})$ versus T^{-1}; in the investigated temperature interval no preference for the T or T^{-1} dependence was found.) Extrapolating the inverse of the forward scattering cross-section to zero yields the mean field estimated spinodal temperature (see Figure 2). All values for the spinodal temperature as a function mixture composition are collected in Table 2. The spinodal data are also presented in Figure 5b. In this figure the experimental data are compared to the calculated spinodal curve, obtained from the Flory–Huggins expression, eqs 7 and 8, which is discussed below.

Flory–Huggins Interaction Function. In a further analysis the free enthalpy of mixing expression of the Flory–Huggins (FH) theory, eq 7, was used in conjunction with a cubic dependence on the composition

Table 2. Spinodal Temperatures, T_{spin}, Determined from Extrapolation of $[\partial^2\Delta G/(NkT)]/\partial\phi_2^2$ vs T to 0 as a Function of the Mixture Composition

w_{PVME}	T_{spin}/K	estimated uncertainty/K	w_{PVME}	T_{spin}/K	estimated uncertainty/K
0.1	306.25	0.03	0.5	305.15	0.02
0.2	307.35	0.07	0.6	302.8	0.1
0.3	308.32	0.06	0.7	298.47	0.04
0.4	304.37	0.05	0.8	305.2	0.3

Table 3. Values of the Parameters in the Composition- and Temperature-Dependent Interaction Parameter Given by Eq 8 Obtained from the Compositional Curvature of the Gibbs Energy Derived from the Forward Scattering Cross-Sections[a]

g_{ij}	value in eq 8	estimated uncertainty	g_{ij}	value in eq 8	estimated uncertainty
g_{00}	−0.1039	0.0014	g_{20}	−0.3454	0.0003
g_{01}	0.00328 K^{-1}	0.000005 K^{-1}	g_{21}	0.00053 K^{-1}	0.00003 K^{-1}
g_{10}	−0.131	0.003	g_{30}	3.242	0.008
g_{11}	0.00219 K^{-1}	0.00001 K^{-1}	g_{31}	−0.00830 K^{-1}	0.00003 K^{-1}

[a] The parameter values have been obtained from a fit of the available experimental data excluding the data for which the residual background intensity is larger than 5% of the determined forward scattering cross-section.

(eq 8a) for the interaction parameter function and a linear temperature dependence for the coefficients g_i (eq 8b). The fit was performed on the second-order compositional derivative of the extended Flory−Huggins interaction parameter $g(\phi_2,T)$ calculated from the scattering cross-sections

$$g''(\phi_2,T) \equiv \frac{\partial^2 g(\phi_2,T)}{\partial {\phi_2}^2} = -\frac{1}{2}\left(\frac{V_0}{\bar{b}^2}\left(\frac{\partial\sigma}{\partial\Omega}(q=0)\Big|_{conc}\right)^{-1} - \frac{1}{s_1\phi_1} - \frac{1}{s_2\phi_2}\right) \quad (9)$$

The polynomial coefficients are summarized in Table 3. Again, from the available temperature range we are unable to distinguish the exact temperature dependence and both a linear and a reciprocal temperature function accurately fit the data. To investigate the temperature dependence in more detail, additional data covering a larger temperature interval are required.

The concentration dependence of $g''(\phi_2,T)$is presented in Figure 3a at two different temperatures. The temperature dependence at constant mixture composition is presented in Figure 3b. Using the cubic polynomial (eq 8) the composition dependence of $g''(\phi_2,T)$ is fitted quite accurately up to compositions $w_{PVME} \approx 0.7$ and for higher polymer concentrations $g(\phi_2,T)$ is slightly underestimated. To improve the data fitting also for these high compositions one may try a polynomial expansion of even higher order in ϕ_2. Unfortunately including in $g(\phi_2,T)$ powers at concentrations higher than $l_{max} = 3$ does not really improve the results. In fact, the number of coefficients becomes too large, and correlations between the coefficients turn out to be problematic, resulting in fits with undesirable variations in composition and temperature between data points. Therefore, we accept the deviations in the high composition range, and we will comment on this when we compare the experimental and predicted phase behavior. The underestimation of $g(\phi_2,T)$ at higher polymer compositions is also visible in Figure 3b, representing the temperature dependence. In Figure 3c we present the difference between the experimental and fitted

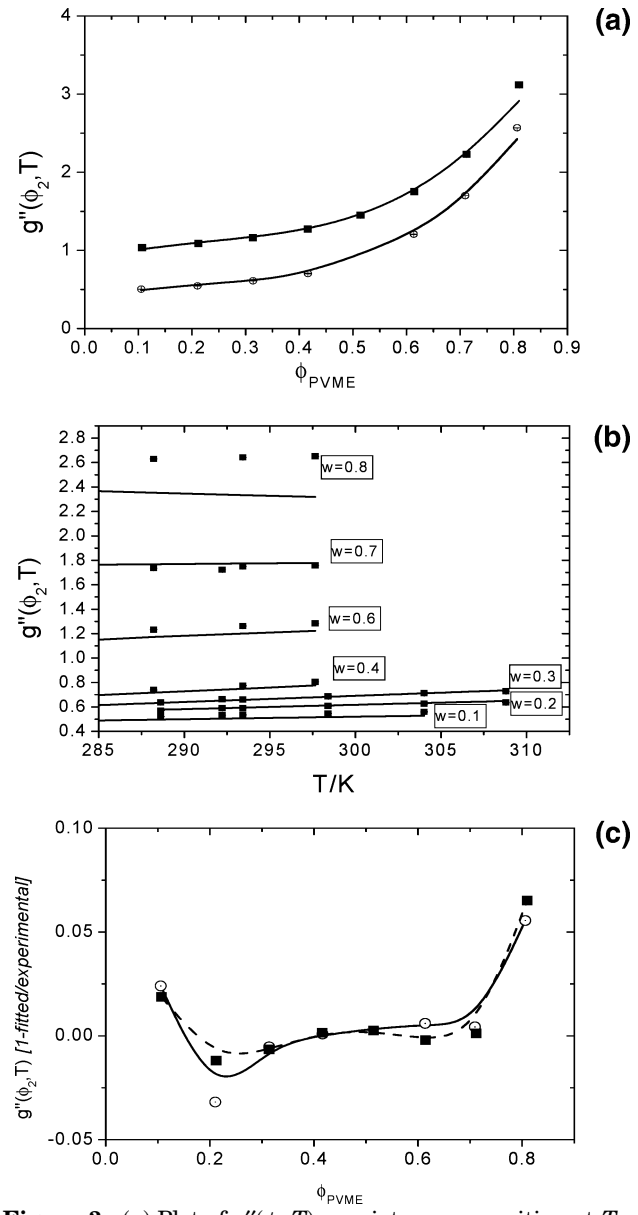

Figure 3. (a) Plot of $g''(\phi_2,T)$ vs mixture composition at T = 288.2 (○) and 293.4 K (■). Solid lines are the result of the polynomial fit. (b) Plot of $g''(\phi_2,T)$ vs temperature at given mixture compositions ($w_{PVME} = w$). Solid lines are the result of the polynomial fit. (c) Plot of $g''(\phi_2,T)$ (1 − fitted/experimental) composition at T = 288.2 (○) and 293.4 K (■) using the polynomial fit.

values of $g''(\phi_2,T)$ as a function of composition for the same temperatures shown in Figure 3a. Clearly, the deviations are systematic, showing the same course for both temperatures, indicating that the polynomial fit is in fact unable to quantitatively represent the temperature and compositional dependence of the experimental data. Of course, in principle, a properly selected polynomial expansion for $g''(\phi_2,T)$ should be able to capture the data quantitatively if we take a sufficient number of coefficients. However, as we noticed, a practical problem arises: the limited number of experimental data points and their limited experimental accuracy put restrictions on how many polynomial coefficients can be determined with sufficient accuracy without also running into problems with the correlations between parameters.

The problems associated with the polynomial functions, eq 8, are further illustrated in Figure 4. In this

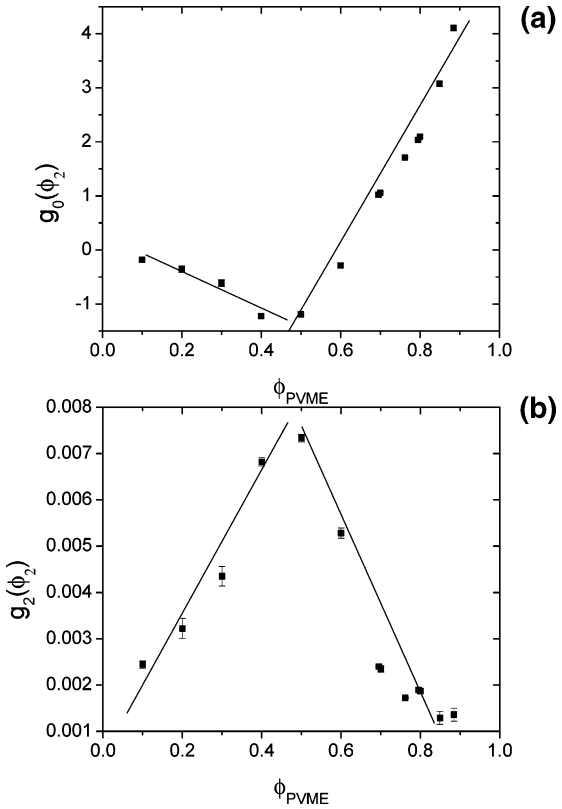

Figure 4. Plot of g_0 (a) and g_2 (b) as a function of mixture composition, obtained from fitting the data at constant composition with a linear temperature function. The solid lines are drawn to guide the eye.

figure the result of a different fitting procedure is presented. Instead of fitting the experimental data simultaneously, the temperature dependence for each mixture composition was first fitted with a linear temperature function $g(T) = g_0 + g_2 \cdot T$ with g_0 and g_2 constants. For each composition an excellent T-fit is obtained with values for g_0 and g_2 varying with composition. The composition dependence of the coefficients g_0 and g_2 is presented in Figure 4, and for both coefficients two approximately linear composition-dependent regimes of opposite slope and meeting at $w_{PVME} \approx 0.5$ can be discerned. In what follows we will use eq 8 in combination with the parameter values given in Table 3 to predict other thermodynamic properties for the system PVME/D_2O.

Predicted LCST Phase Behavior. Equations 7 and 8 are valid for solutions of a monodisperse polymer in a single solvent and are used to predict the LCST phase behavior of PVME/D_2O. Spinodal, coexistence curves, critical conditions, as well as the liquid−liquid−liquid (L−L−L) three-phase equilibrium line are calculated and depicted in Figure 5a using the polynomial function. The predicted spinodal curve is compared with the experimental spinodal data, determined directly from SANS. In Figure 5a and b the predicted phase behavior for PVME/D_2O can be compared to the experimental phase diagram of PVME/H_2O: in particular, cloud point data determined independently by cloud point measurements using SALLS and DSC[14,51] and the three-phase line estimated from DSC data as discussed earlier.[51]

Due to the polydispersity of the PVME sample, the experimental cloud point data are not coexistence data and cannot therefore strictly be compared quantitatively to the predicted binodal, calculated for a monodisperse

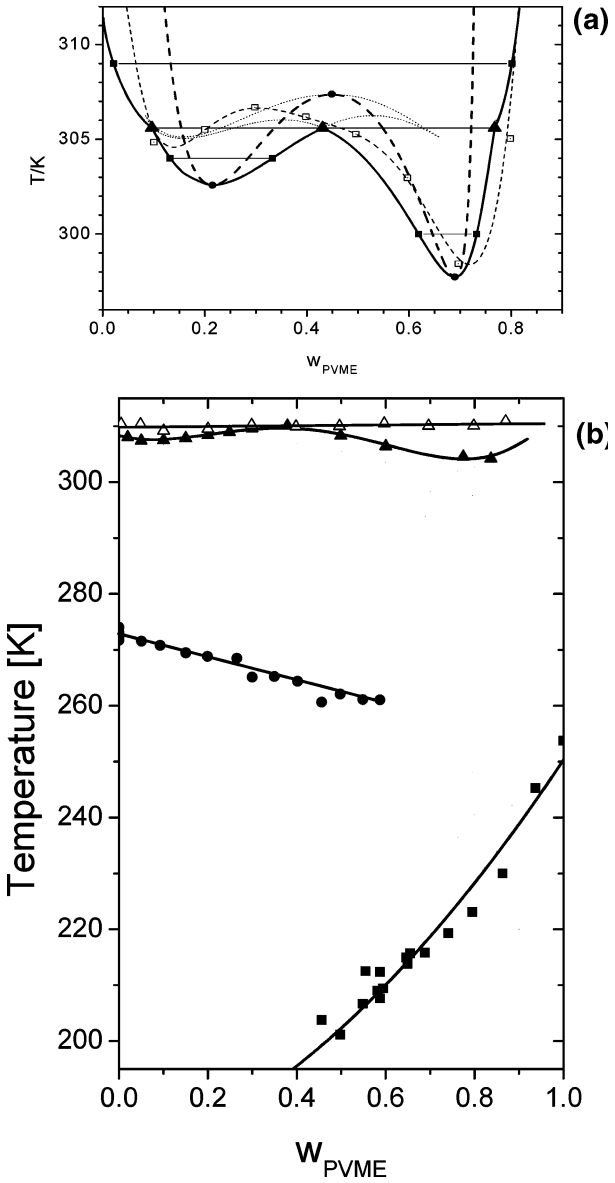

Figure 5. (a) Temperature−composition phase diagram at atmospheric pressure of PVME/D_2O. Experimentally estimated spinodal temperatures (□, ---); predicted spinodal curve (---), predicted binodal curve (—), predicted critical points (●), predicted three-phase line (▲−▲−▲), predicted two-phase tie lines (■−■); metastable and unstable extensions of coexistence lines are depicted by dotted lines. The predictions are based on the cubic polynomial interaction function in eq 8. (b) Temperature−composition phase diagram of PVME/H_2O showing the experimental LCST cloud point curve (▲), the experimentally estimated three-phase line (△), the melting point line of water (●), and the glass transition of PVME/H_2O (■) as a function of composition. Data are taken from the literature, and lines are drawn to guide the eye.[52]

polymer.[50] Nevertheless, using eq 8 for the interaction function the binodal curve compares favorably and qualitatively with the experimental cloud point data as the shape and bimodality of the binodal curve is predicted in agreement with the experimental results. Also, the predicted spinodal curve is in qualitative agreement with the spinodal points directly extrapolated from the scattering cross-sections. However, it is disappointing to see that the predicted LCST spinodal deviates considerably from the directly determined spinodal conditions based on the cubic composition polynomial even though only a relatively short extrapo-

lation is required. Also, in the water-rich part of the phase diagram the difference between the calculated spinodal and binodal and the experimental data is about 5 °C. These deviations are related to the inability to accurately fit the experimental scattering cross-sections with the extended Flory−Huggins interaction function (eq 8).

Summarizing, the predicted phase behavior is in qualitative agreement with the experimental data, and importantly the unusual bimodal phase behavior (called type 3 in the literature)[14,17] is predicted. However, quantitative agreement is not reached, which can be traced back to the inability to quantitatively fit the values of $g''(\phi_2,T)$ with the polynomial functions. This can only be resolved by either having more experimental data or using a theoretical approach that explains the complicated temperature and composition dependencies based on the molecular properties of the system PVME/$H_2O(D_2O)$. It should be noted that the bimodal phase behavior is not caused by the rather broad molar mass distribution of the polymer sample (typically $M_w/M_n \approx 1.5$ for these commercial PVME samples). In fact, recent experiments on carefully synthesized $M_w/M_n \approx 1.05-1.10$ as well as further fractionated PVME samples show the same bimodal phase behavior independent of the PVME polydispersity.[53]

Ornstein−Zernike Correlation Length in the Concentrated Regime. Much has been said about the dependence of the correlation length on temperature and concentration in the dilute, semidilute, and concentrated regimes of the polymer/solvent phase diagram.[54−61] Some of our data are located at the end of the semidilute regime, but most data are in the concentrated regime, and for certain temperatures the conditions as a function of composition may change from good solvent to Θ-solvent conditions depending on the temperature distance to the miscibility gap, and the correlation length will change accordingly. Therefore, it is difficult to analyze or interpret the data that we have in the perspective of scaling theories. However, the data can be set in the context of a general relationship between the correlation length and the amplitude of the thermal concentration fluctuations as pioneered by Debye and further elaborated by others. In the mean field approximation the following sum rule applies[35,56,60]

$$\xi^2 = \xi_0^2\left(\frac{\partial^2 \Delta G/(NkT)}{\partial \phi_2^2}\right)^{-1} \qquad (10)$$

with ξ_0 being the critical correlation amplitude.

In Figure 6 the correlation length is presented according to eq 10 in a double-logarithmic plot and is indeed found to be proportional to the compositional curvature. For sufficiently small values of the Gibbs curvature large correlation lengths are obtained and all data roughly coincide and are in agreement with eq 10. However, for smaller correlation lengths connected with smaller amplitudes of the concentration fluctuations the situation is not as simple as that predicted by eq 10: Data for different concentrations and different temperatures appear to cluster together on three distinct power law dependencies. In the composition interval $0.75 \le w_{PVME} \le 0.85$ the data all follow eq 10. However, in the range $0.1 \le w_{PVME} \le 0.7$ the data cluster on two separate straight lines. On the basis of the data in Figure 6, three separate straight lines were drawn manually as shown and the exponents were estimated.

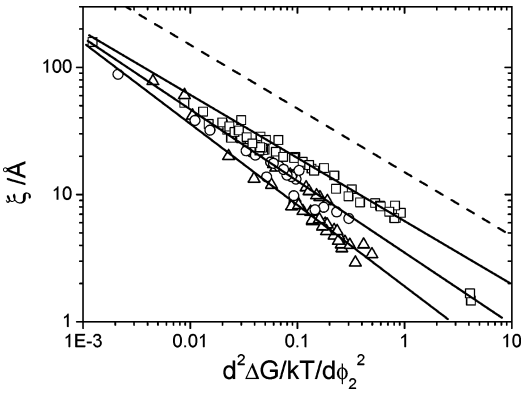

Figure 6. Double-logarithmic plot of the correlation length ξ vs $\partial^2[\Delta G/(NkT)]/\partial\phi_2^2$: (□) $0.75 \le w_{PVME} \le 0.85$, (○) $0.6 \le w_{PVME} \le 0.7$, (△) $0.1 \le w_{PVME} \le 0.5$. The solid lines are drawn to guide the eye. Three separate straight lines were drawn by hand as shown, and the exponents in $\xi \approx (\partial^2[\Delta G/(NkT)]/\partial\phi_2^2)^{-\eta}$ were estimated. The dashed line is the scaling relation with $\eta = 1/2$.

Although the correlation lengths are still proportional to the amplitude of the thermal composition fluctuations, a different exponent is found, i.e., $\xi^2 = \xi_0^2(\partial^2[\Delta G/(NkT)]/\partial\phi_2^2)^{-\eta}$ with $\eta \approx 0.6$ in the range $0.6 \le w_{PVME} \le 0.7$ and for $w_{PVME} = 0.1$ and $\eta \approx 0.55$ in the range $0.2 \le w_{PVME} \le 0.5$. Thus far this peculiar dependence of the correlation length is not understood.

Complex Formation in Concentrated Mixtures. Finally, we return to the issue of the formation of PVME/water complexes. According to eq 5 $\partial^2[\Delta G/(NkT)]/\partial\phi_2^2$ is a quantitative measure for the average amplitude of the spontaneous thermal composition fluctuations $\langle\Delta\phi_2^2\rangle$ in the homogeneous mixture and conversely is also a measure for the energy (in units of *kT)* stored in the spontaneous fluctuations or, alternatively, a measure for the energy required to create a concentration fluctuation of average amplitude $\langle\Delta\phi_2^2\rangle$. The larger the value of $(\partial^2\Delta G/NkT/\partial\phi_2^2)$, the smaller the amplitude of the spontaneous composition fluctuations becomes on average (eq 5). In homogeneous mixtures with normal solution behavior, in which no complex formation occurs (e.g., solutions of polystyrene in cyclohexane or in DOP), a typical concave dependence on mixture composition is found for $(\partial^2\Delta G/NkT/\partial\phi_2^2)$, with large positive values at the extremes of the composition interval and reaching its minimum at some intermediate mixture composition. The high values at the extremes of the composition interval indicate that it becomes gradually more difficult for these concentrations to induce large composition fluctuations in a normal mixture. In fact, in the pure component only density fluctuations are possible; the scattered intensity due to concentration fluctuations is zero, and correspondingly $(\partial^2\Delta G/NkT/\partial\phi_2^2)$ becomes infinite.

The situation is quite different in PVME/water mixtures. In Figure 7 $(\partial^2\Delta G/NkT/\partial\phi_2^2)$ is plotted as a function of composition at several temperatures for PVME/D_2O mixtures. Just as for normal solution behavior, the compositional curvature increases rapidly at very high polymer concentration, indicating that it becomes gradually more difficult to induce large composition fluctuations in these highly concentrated polymer mixtures. In Figure 7 the expected upswing at the dilute polymer side of the diagram is not observed because the smallest investigated polymer composition, $w_{PVME} = 0.1$, is not small enough to observe this

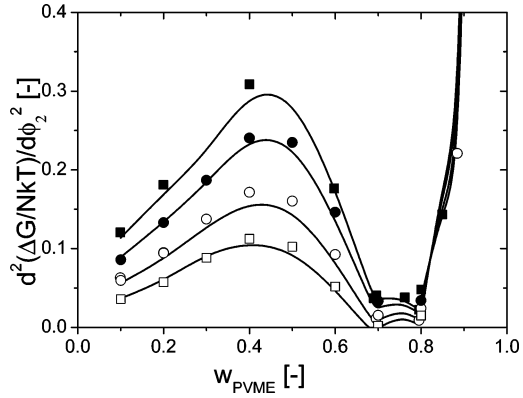

Figure 7. Plot of $[\partial^2\Delta G/(NkT)]/\partial\phi_2^2$ vs mixture composition at indicated temperatures: T = (■) 283, (●) 288, (○) 293, and (□) 298 K.

phenomenon. However, interestingly and most importantly, $(\partial^2\Delta G/NkT/\partial\phi_2^2)$ does not show the typical concave dependence expected for normal solution behavior but reaches a maximum in the interval $0.3 \leq w_{PVME} \leq 0.5$. This thus indicates that at these intermediate compositions it again becomes more difficult to induce composition fluctuations. Thus, the experimental data reveal that at intermediate compositions the amplitude of the thermal compositional fluctuations decreases, which can point to complexation of PVME and D_2O.

The maximum value of $\partial^2\Delta G/NkT/\partial\phi_2^2$ is higher the lower the temperature, but notwithstanding this increase, even at the lowest investigated temperature the energy needed to induce the fluctuations is just about $0.3kT$. Thus, the clustering of water and PVME in this composition interval and at the investigated temperature is still small compared to the thermal energy. Therefore, it should be concluded that in the temperature interval considered in this study the specific interactions between water/D_2O and PVME are still too weak to speak about the formation of a complex in the system. Nevertheless, the maximum value increases with decreasing temperature, and it is conceivable that at lower temperatures a stable complex between water and PVME might be formed. Evidently SANS provides a unique opportunity to investigate the thermal fluctuations, in general, and the presence of association and even complexation, in particular. This will be the topic of a further study using neutron scattering.

Conclusions and Outlook

We reported on SANS measurements for mixtures of PVME and D_2O covering the whole composition range in the homogeneous part of the phase diagram bounded by the LCST at high temperature and the crystallization of D_2O at low temperatures. The raw SANS data were treated according to fluctuation theory to obtain the absolute scattering cross-section for concentration fluctuations. These data were fitted by the OZ equation, yielding the absolute scattering cross-section in the forward direction and the Ornstein−Zernike correlation length as a function of temperature and composition. The forward absolute scattering cross-sections were converted in values for the compositional curvature of the Gibbs' energy.

Independent of any (molecular) model spinodal temperatures were determined from the experimental values of the compositional curvature of the 'Gibbs' energy. These values were also used to obtain values for the polynomial coefficients in extended FH interaction functions, $g(\phi_2,T)$, depending linearly on temperature and cubicly on mixture composition. At higher compositions the agreement between experimental data and fit becomes lower. Including in $g(\phi_2,T)$ higher powers in concentration did not improve the agreement between fit and experiment, mainly due to correlations between the coefficients. The problems associated with the polynomial functions were further illustrated; using a different fitting procedure it was found that the composition dependence is difficult to fit with a smooth polynomial but would be better described by two approximately linear composition-dependent regimes of opposite slope and meeting at about $w_{PVME} \approx 0.5$.

The extended FH interaction function was used to predict the thermodynamic properties of the system. Spinodal, coexistence curves, critical conditions, as well as the liquid−liquid−liquid (L−L−L) three-phase equilibrium line were predicted and are in qualitative agreement with the experimental data, and importantly the unusual bimodal phase behavior[17] was predicted. The dependence of the correlation length ξ on temperature and concentration was shown to follow power law behavior $\xi^2 \approx [(\partial^2\Delta G/(NkT)]/\partial\phi_2^2)^{-\eta}$ with the exponent η depending on the composition (interval). Thus far the peculiar dependence of the exponent η on composition is not understood, and further investigation is required to understand it.

Finally, the issue of the formation of PVME/water complexes was discussed. On the basis of the values of the molar mass of PVME determined in D_2O and toluene-d_8, it was concluded that in dilute solutions at 20 °C no stable molecular complex between D_2O and PVME is formed. Also, in the concentrated polymer mixtures the scattering results do not provide evidence for strong complex formation. Even at the lowest investigated temperature the energy needed to induce compositional fluctuations was found to be only ca. $0.3kT$, and in the temperature interval considered in this study, the specific interactions between water/D_2O and PVME are too weak to bring about the formation of a complex in the system.

Evidently SANS provides a unique opportunity to investigate the thermal fluctuations and the presence of association and even complexation. It will be of interest to investigate mixtures of PVME/D_2O at lower temperatures than investigated so far and determine if the amplitude of the compositional fluctuations will decrease further so that we can interpret the SANS experiments in terms of complex formation between polymer and solvent. Measurements at lower temperatures are possible for highly concentrated mixtures, as it is possible to prevent the crystallization of D_2O at high polymer concentrations.

Furthermore, from a theoretical viewpoint it will be of interest to investigate if the complicated phase behavior and the detailed information obtained from the SANS scattering experiments can be understood using a theoretical approach that incorporates directly and explicitly the formation of hydrogen-bonding interactions.

Acknowledgment. We thank the Dutch Science Foundation (NWO) for financial support in the application for beam time at ISIS. Peter Maris, Bert Berge, and Frank Meeussen are acknowledged for sample preparation and assistance in the SANS measurements. This

work was supported by the bilateral (international) scientific and technological cooperation of the Ministry of the Flemish Community and the Ministry of Science and Technology of the People Republic of China (BIL01/06). The authors thank the Funds for Scientific Research Flanders (FWO) and IUAP5/03 (Belgian Program on Inter University Attraction Poles initiated by the Belgian State Prime Ministers office) for financial support. P.M. and F.M. are indebted to the Flemish Institute for the promotion of Scientific-Technological Research in Industry (IWT) for a fellowship.

Supporting Information Available: Information to calculate volume fractions and scattering lengths, the numerical values of SANS scattering cross-sections for concentration fluctuations $\partial\sigma/\partial\Omega(0)|_{conc}$, correlation length ξ, and residual background B at investigated temperatures and mixture compositions; estimated uncertainties $SD_{\partial\sigma/\partial\Omega(0)|conc}$ and SD_{ξ} are also provided. This material is available free of charge via the Internet at http://pubs.acs.org.

References and Notes

(1) Walker, J. S.; Vause, C. A. *Proceedings of the 8th Symposium on Thermophysical Properties*; American Society of Mechanical Engineers: New York, 1982; vol. 1, pp 411−418.
(2) Walker, J. S.; Vause, C. A. *Phys. Lett. A* **1980**, *79A* (5−6), 421−424.
(3) Dormidontova, E. E. *Macromolecules* **2002**, *35* (3), 987−1001.
(4) Panayiotou, C.; Sanchez, I. C. *Macromolecules* **1991**, *24* (23), 6231−6237.
(5) Tanaka, F. *Polym. J. (Tokyo, Jpn.)* **2002**, *34* (7), 479−509.
(6) Saeki, S.; Kuwahara, N.; Nakata, M.; Kaneko, M. *Polymer* **1976**, *17* (8), 685−689.
(7) Molyneux, P. Synthetic polymers. In *Water Comprehensive Treatise*; Franks, F., Ed.; Plenum Press: New York, 1975; Vol. 4, pp 569−757.
(8) Meeussen, F.; Nies, E.; Berghmans, H.; Verbrugghe, S.; Goethals, E.; Du Prez, F. *Polymer* **2000**, *41* (24), 8597−8602.
(9) Rehage, G. *Kunststoffe* **1963**, *53*(9), 605−614.
(10) Sanchez, I. C.; Lacombe, R. H. *Macromolecules* **1978**, *11* (6), 1145−1156.
(11) Kleintjens, L. A.; Koningsveld, R. Mean-field lattice-gas description of fluid-phase equilibria. In *Chemical Engineering in Supercritical Fluid Conditions*; Paulaitis, M. E., Ed.; Ann Arbor Science: Ann Arbor, Michigan, 1983; pp 245−262.
(12) Nies, E.; Stroeks, A. The Simha-Somcynsky hole theory: thermodynamic properties based on compositional derivatives. In *Integration of Fundamental Polymymer Science and Technology*; Kleintjens, L. A., Lemstra, P. J., Elsevier Applied Science, 1988; pp 231−237.
(13) Stroeks, A.; Nies, E. *Macromolecules* **1990**, *23* (18), 4092−4098.
(14) Schaefer-Soenen, H.; Moerkerke, R.; Berghmans, H.; Koningsveld, R.; Dusek, K.; Solc, K. *Macromolecules* **1997**, *30* (3), 410−416.
(15) Maeda, Y.; Mochiduki, H.; Yamamoto, H.; Nishimura, Y.; Ikeda, I. *Langmuir* **2003**, *19* (24), 10357−10360.
(16) Tanaka, H. *AIP Conf. Proc.* **1992**, *256* (Slow Dyn. Condens. Matter), 238−239.
(17) Solc, K.; Dusek, K.; Koningsveld, R.; Berghmans, H. *Collect. Czech. Chem. Commun.* **1995**, *60* (10), 1661−1688.
(18) Huggins, M. L. *J. Chem. Phys.* **1942**, *9*, 440.
(19) Flory, P. J. *J. Chem. Phys.* **1942**, *9*, 660.
(20) Dudowicz, J.; Freed, K. F. *Macromolecules* **1991**, *24* (18), 5076−5095.
(21) Chatterjee, A. P.; Schweizer, K. S. *Macromolecules* **1998**, *31* (7), 2353−2367.
(22) Hammouda, B.; Ho, D.; Kline, S. *Macromolecules* **2002**, *35* (22), 8578−8585.
(23) MacKenzi, A. P.; Rasmussen, D. H. In *Water Structure at the Polymer−Water Interface*; Jellinek, H. H. G., Ed.; John Wiley: New York, 1972.
(24) De Dood, M. J. A.; Kalkman, J.; Strohhofer, C.; Michielsen, J.; Van der Elsken, J. *J. Phys. Chem. B* **2003**, *107*, 5906.
(25) Meeussen, F.; Bauwens, Y.; Moerkerke, R.; Nies, E.; Berghmans, H. *Polymer* **2000**, *41* (10), 3737−3743.
(26) Zhang, J.; Berge, B.; Meeussen, F.; Nies, E.; Berghmans, H.; Shen, D. *Macromolecules* **2003**, *36* (24), 9145−9153.
(27) Maeda, H. *Macromolecules* **1995**, *28* (14), 5156−5159.
(28) Maeda, Y. *Langmuir* **2001**, *17* (5), 1737−1742.
(29) Maeda, H. *J. Polym. Sci., Part B: Polym. Phys.* **1994**, *32* (1), 91−97.
(30) Mueller, E. A.; Gubbins, K. E. *Ind. Eng. Chem. Res.* **2001**, *40* (10), 2193−2211.
(31) Wertheim, M. S. *J. Stat. Phys.* **1984**, *35*, 19.
(32) Veytsman, B. A. *J. Phys. Chem.* **1990**, *94* (23), 8499−8500.
(33) Afroze, F.; Nies, E.; Berghmans, H. *J. Mol. Struct.* **2000**, *554* (1), 55−68.
(34) Moerkerke, R.; Koningsveld, R.; Nies, E.; Berghmans, H.; Dusek, K.; Solc, K. *Wiley Polymer Networks Group Review Series* **1998**, *1* (Chemical and Physical Networks), 463−473.
(35) Debye, P. *J. Chem. Phys.* **1959**, *31*, 680−687.
(36) Higgins, J. S.; Benoit, H. C. *Polym. Neutron Scattering* 1994, Clarendon Press: Oxford, U.K.
(37) Takada, M.; Okano, K.; Kurita, K.; Furusaka, M. *Kobunshi Ronbunshu* **1994**, *51* (11), 689−693.
(38) Okano, K.; Takada, M.; Kurita, K.; Furusaka, M. *Polymer* **1994**, *35* (11), 2284−2289.
(39) An, S. W.; Thomas, R. K.; Forder, C.; Billingham, N. C.; Armes, S. P.; Penfold, J. *Langmuir* **2002**, *18* (13), 5064−5073.
(40) Jinnai, H.; Smalley, M. V.; Hashimoto, T.; Koizumi, S. *Langmuir* **1996**, *12* (5), 1199−1203.
(41) Heenan, R. K.; King, S. M. http://www.isis.rl.ac.uk/largescale/loq/documents/techspec.doc; 2003.
(42) King, S. M.; Heenan, R. K. *Using COLETTE;* http://www.isis.rl.ac.uk/largescale/loq/documents/using_colette.doc; RAL-95-005; 1-1-1995.
(43) Smoluchowski, M. *Ann. Phys. (Berlin, Germany)* **1908**, *25*, 205.
(44) Einstein, A. *Ann. Phys. (Berlin, Germany)* **1911**, *33*, 1275−1298.
(45) Chu, B. *J. Chem. Phys.* **1963**, *41* (1), 226−234.
(46) King, S. M. *Small Angle Neutron Scattering*; http://www.isis.rl.ac.uk/largescale/loq/documents/sans.htm; 1-12-1995.
(47) Bhatia, A. B.; Thornton, D. E. *Phys. Rev. B: Solid State* **1970**, *2* (8), 3004−3012.
(48) Tolman, R. C. *The Principles of Statistical Mechanics* 1955, Oxford University Press: Oxford, U.K.
(49) Hill, T. L. *An Introduction to Statistical Thermodynamics*; 1960, Addison-Wesley: London, U.K.
(50) Koningsveld, R.; Stockmayer, W. H.; Nies, E. *Polymer Phase Diagrams: A Textbook*; 2001, Oxford University Press: Oxford, U.K.
(51) Meeussen, F. Ph.D. Thesis, K. U. Leuven, 2002.
(52) Meeussen, F.; Bauwens, Y.; Moerkerke, R.; Nies, E.; Berghmans, H. *Polymer* **2000**, *41* (10), 3737−3743.
(53) Manuscript in preparation.
(54) Cotton, J. P.; Nierlich, M.; Boue, F.; Daoud, M.; Farnoux, B.; Jannink, G.; Duplessix, R.; Picot, C. *J. Chem. Phys.* **1976**, *65* (3), 1101−1108.
(55) Sanchez, I. C. *J. Phys. Chem.* **1989**, *93* (19), 6983−6991.
(56) Anisimov, M. A.; Kiselev, S. B.; Sengers, J. V.; Tang, S. *Physica A* **1992**, *188* (4), 487−525.
(57) Wiltzius, P.; Haller, H. R.; Cannell, D. S. *Phys. Rev. Lett.* **1983**, *51* (13), 1183−1186.
(58) Geissler, E.; Mallam, S.; Hecht, A. M.; Rennie, A. R.; Horkay, F. *Macromolecules* **1990**, *23* (25), 5270−5273.
(59) Chatterjee, A. P.; Schweizer, K. S. *Macromolecules* **1999**, *32* (3), 923−934.
(60) Dudowicz, J.; Freed, K. F.; Douglas, J. F. *J. Chem. Phys.* **2002**, *116* (22), 9983−9996.
(61) Eu, B. C.; Gan, H. H. *J. Chem. Phys.* **1995**, *102* (1), 585−604.

MA0485641